Small-Angle Neutron Scattering Study of Mixtures of Cationic Polyelectrolyte and Anionic Surfactant: Effect of Polyelectrolyte Charge Density

L. Magnus Bergström,* U. R. Mikael Kjellin, and Per M. Claesson

Department of Chemistry, Surface Chemistry, Drottning Kristinas väg 51, Royal Institute of Technology, SE-100 44 Stockholm, and YKI, Institute for Surface Chemistry, Box 5607, SE-114 86 Stockholm, Sweden

Isabelle Grillo

Institut Laue-Langevin (ILL), DS/LSS, 6, rue Jules Horowitz, B.P. 156, 38042 Grenoble Cedex, France

Received: August 28, 2003; In Final Form: November 26, 2003

We have studied mixtures of an anionic surfactant (deuterated sodium dodecyl sulfate, SDS-*d*) and cationic polyelectrolytes with different charge densities (10%, 30%, 60%, and 100%) using small-angle neutron scattering (SANS). Near compositions corresponding to charge neutralization, the solutions phase separate into a complex phase (precipitate) consisting of, in the cases of 30%, 60%, and 100% charge density, a two-dimensional (2D) hexagonal lattice of close-packed cylindrical micelles and a clear liquid. When either polyelectrolyte with charge density less than 100% or SDS-*d* is present in sufficient excess, the solution becomes clear and isotropic, and from the scattering data we may conclude that prolate or rod-shaped micelles are present. The micelles are seen to grow in length with increasing SDS-*d* concentration and polyelectrolyte charge density from about 80 Å to 550 Å, whereas the cross-sectional radius is 15 Å and approximately constant. The number of micelles per polyelectrolyte chain is found to be slightly larger than unity (1−6). In some of the (turbid) samples rod-shaped micelles are found to coexist with larger polyelectrolyte−surfactant complexes. Solutions consisting of 10% charged polyelectrolyte and SDS-*d* are very viscous and gellike, and the complex phase is much less defined with a much larger distance between adjacent aggregates in the complex phase.

Introduction

The association between polyelectrolytes and oppositely charged surfactants has been extensively studied in recent years, both in bulk and at interfaces, using a wide range of different techniques.[1−7] It has in general been found that the addition of a polyelectrolyte has a large impact on the association behavior in solutions containing an oppositely charged surfactant. For example, the surfactant concentration at which this cooperative association step occurs, the critical association concentration (cac), is generally much lower than the critical micelle concentration (cmc), and it decreases with increasing charge density of the polyelectrolyte.

Also, the phase behavior appears to be unusually rich with a strong dependence on both surfactant and polyelectrolyte architecture and concentration. On the basis of different techniques, several structures of polyelectrolyte−surfactant complexes have been proposed depending on the system under investigation. For instance, Cosgrove et al.[8] studied complexes between gelatin and sodium dodecyl sulfate (SDS) and concluded from small-angle neutron scattering (SANS) measurements that globular micelle-like structures were formed along the polyelectrolyte chain in a bead-and-necklace structure, that is, in a similar arrangement as that for the well-characterized complexes formed between uncharged poly(ethylene oxide) and SDS.[9,10] On the other hand, Antonietti and co-workers found from wide-angle X-ray studies that in several polyelectrolyte−surfactant systems ordered mesomorphous phases with rather complex topology were present.[11−15] More recently, lamellar, 2-dimensional (2D) hexagonal as well as various cubic liquid-crystalline structures have been observed from small-angle X-ray scattering (SAXS) measurements of mixtures of cationic polyelectrolyte (starch) and anionic surfactant[16] as well as anionic polyelectrolyte and cationic surfactant.[17−19] Lamellar, 2D hexagonal or 2D distorted hexagonal complex phases were seen to form in mixtures of polyvinylamine and various sodium alkyl sulfates depending on pH and surfactant chain length.[20]

We have recently investigated aqueous mixtures of the cationic polyelectrolyte poly{(2-propionyloxy)ethyl} trimethylammonium chloride (PCMA) and the (deuterated) anionic surfactant SDS-*d* with small-angle neutron scattering (SANS).[21] After the samples were mixed, a phase separation into a white precipitate and a transparent water solution occurred for samples with a ratio $r \equiv$ [total charge of SDS-*d*]/[total charge of polyelectrolyte] = 0.25−1.5. We studied the samples in pure D_2O, where SDS-*d* is contrast matched, as well as in a D_2O/H_2O mixture, which corresponds to the contrast match point of the polyelectrolyte. For both solvents a sharp but resolution-limited peak from the PCMA−SDS-*d* complex appears in the SANS spectra at a scattering vector $q = 0.165$ Å^{-1} corresponding to an interplanar spacing of 38 Å. The modulus of the scattering vector q is given by $q = 4\pi \sin\theta/\lambda$, where 2θ is the angle between the direct and scattered beam and λ is the neutron wavelength. At low q values the scattering intensity decays as $I \propto q^{-4}$ characteristic of sharp interfaces (Porod's law) and demonstrates the presence of a three-dimensional structure which is consistent with the formation of a precipitate that may be observed with the bare eye.

* Author to whom correspondence should be addressed. Fax: +46 8 20 89 98. E-mail: magnus.bergstrom@surfchem.kth.se.

10.1021/jp036562x CCC: $27.50
Published on Web 01/16/2004

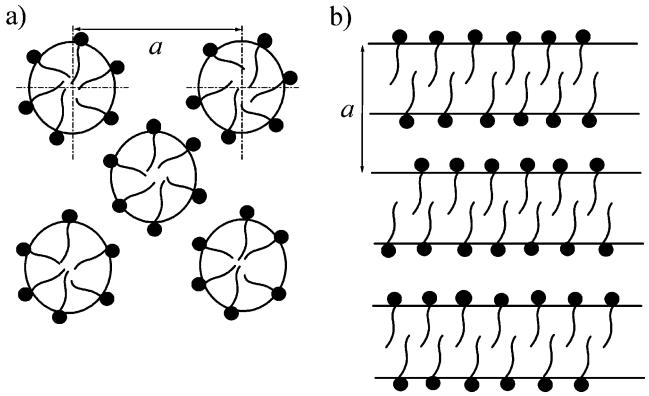

Figure 1. Schematic representations of (a) the 2D hexagonal structure of cylindrical surfactant micelles and (b) the 1D lamellar structure of surfactant bilayers with an aqueous region separating the hydrophobic cores. The polyelectrolyte must either be located in the aqueous region or, possibly, be partitioned between the hydrophobic and hydrophilic regions.

A similar phase separation into a solid phase and an isotropic liquid was also seen in mixtures of SDS and the 100% charged polyelectrolyte polyvinylamine (PVAm) and poly{3-(2-methylpropionamido)propyl}trimethylammonium chloride (MAPTAC). To investigate the internal structure of the solid phase in more detail, we studied the complex phases with SAXS.[22] We found that in charge-neutralized mixtures of either MAPTAC or PCMA, that is, linear polyelectrolytes with short side chains, with SDS a 2-dimensional hexagonal structure was present, whereas a mixture of a linear 100% charged polyelectrolyte without side chains (PVAm) with SDS formed a lamellar structure. We concluded that the cylinders in the hexagonal structure and the bilayers in the lamellar structure are based on self-assembled surfactant aggregates with the polyelectrolyte mainly located in the aqueous region adjacent to the charged surfactant headgroups (cf. Figure 1). We may note that our result of a lamellar structure of PVAm−SDS complexes differs from the 2D distorted hexagonal structure observed by Zhou et al.[20] for the same system at $5.9 < \mathrm{pH} < 12.0$. The discrepancy may be caused by the fact that we in ref 22 used a polymer with much larger molar mass ($\langle M_w \rangle = 90$ kg/mol) than was done in ref 20 ($\langle M_w \rangle = 25$ kg/mol).

In the present paper, we follow up our recent studies of mixtures of cationic polyelectrolyte and SDS and focus on the structural behavior of mixtures of SDS-*d* and various polyelectrolytes (acrylamide−MAPTAC (AM−MAPTAC)) with different charge densities as a function of surfactant/polyelectrolyte composition.

Materials and Methods

Materials. The polyelectrolytes used in the present study were poly{3-(2-methylpropionamido)propyl}trimethylammonium chloride (MAPTAC) with a number-averaged molecular weight of 480 kg/mol or 2600 monomer segments per molecule and mixtures of a charged monomer (MAPTAC) and the noncharged monomer acrylamide (AM) so as to give a charge density of 10% (AM−MAPTAC10, 1000 kg/mol or 12 000 monomer segments per molecule), 30% (AM−MAPTAC30, 780 kg/mol or 7400 monomer segments per molecule), and 60% (AM−MAPTAC60, 340 kg/mol or 2400 monomer segments per molecule). The four polyelectrolytes were chosen so as to cover a wide range of different charge densities.

The quaternary ammonium cationic group on the MAPTAC monomer is located on a short side chain (cf. Figure 2).

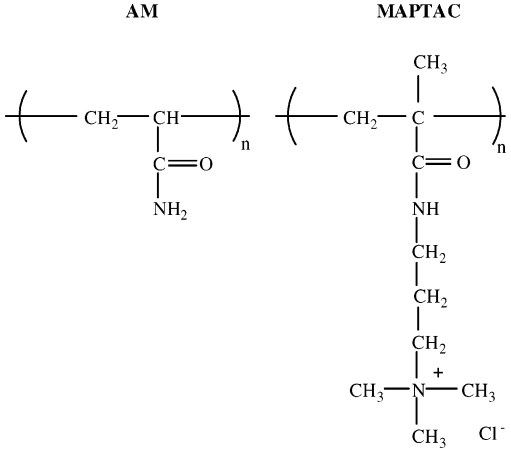

Figure 2. Chemical structure of {3-(2-methylpropionamido)propyl}-trimethylammonium chloride (MAPTAC) and acrylamide (AM).

MAPTAC and the different AM−MAPTAC mixtures were synthesized and kindly provided by the Laboratoire de Physico-Chimie Macromoleculaire, Université Pierre et Marie Curie, Paris. The surfactant, deuterated sodium dodecyl sulfate (SDS-*d*), was obtained from Isotec Inc. (Lot No. EK2050-7) and used without further purification. D_2O was chosen as the solvent in order to minimize the incoherent background from hydrogen and obtain a high scattering contrast with the polyelectrolyte while simultaneously contrast matching the SDS-*d*. In another set of measurements a mixture of H_2O and D_2O was used as the solvent in order to contrast match the polyelectrolyte while yielding a high scattering contrast with SDS-*d*. Accordingly, the molar ratio of the solvent that contrast matched the polyelectrolyte was 86% H_2O and 14% D_2O for MAPTAC, 82% H_2O and 18% D_2O for AM−MAPTAC 60, 77% H_2O and 23% D_2O for AM−MAPTAC30, and 71% H_2O and 29% D_2O for AM−MAPTAC10. All measurements were carried out at 22 °C.

The average excess scattering length density $\Delta\rho$ was calculated using the appropriate molecular volumes and weights of the surfactant monomers: $\Delta\rho_{\mathrm{SDS}-d}$ (D_2O) $= 0.33 \times 10^{10}$ cm^{-2} for SDS-*d* in D_2O, $\Delta\rho_{\mathrm{SDS}-d}$ (mix) $= 6.32 \times 10^{10}$ cm^{-2} for SDS-*d* in a 86/14 H_2O/D_2O mixture (MAPTAC contrast matched), $\Delta\rho_{\mathrm{SDS}-d}$ (mix) $= 6.04 \times 10^{10}$ cm^{-2} for SDS-*d* in a 82/18 H_2O/D_2O mixture (AM−MAPTAC60 contrast matched), $\Delta\rho_{\mathrm{SDS}-d}$ (mix) $= 5.69 \times 10^{10}$ cm^{-2} for SDS-*d* in a 77/23 H_2O/D_2O mixture (AM−MAPTAC30 contrast matched), and $\Delta\rho_{\mathrm{SDS}-d}$ (mix) $= 5.27 \times 10^{10}$ cm^{-2} for SDS-*d* in a 71/29 H_2O/D_2O mixture (AM−MAPTAC10 contrast matched). For the polyelectrolytes in D_2O the following scattering contrasts are valid: $\Delta\rho_{\mathrm{MAPTAC}}$ (D_2O) $= -5.97 \times 10^{10}$ cm^{-2}, $\Delta\rho_{\mathrm{AM-MAPTAC60}}$ (D_2O) $= -5.74 \times 10^{10}$ cm^{-2}, $\Delta\rho_{\mathrm{AM-MAPTAC30}}$ (D_2O) $= -5.36 \times 10^{10}$ cm^{-2}, and $\Delta\rho_{\mathrm{AM-MAPTAC10}}$ (D_2O) $= -4.94 \times 10^{10}$ cm^{-2}.

The samples were prepared by adding a 2 wt % polyelectrolyte stock solution to a surfactant stock solution so as to yield an overall polyelectrolyte concentration of 1 wt % and the desired concentration of SDS-*d*. The samples were measured at least 1 h after preparation. In some mixtures a white precipitate was formed together with an isotropic aqueous phase (cf. Figure 3). Because we did not want to influence the internal structure of the precipitate, those samples were measured without any further treatments such as centrifugation or drying. Nevertheless, two samples were centrifuged and the isotropic liquid phase measured showing that small amounts of large objects were still present. This proves that small particles from the solid

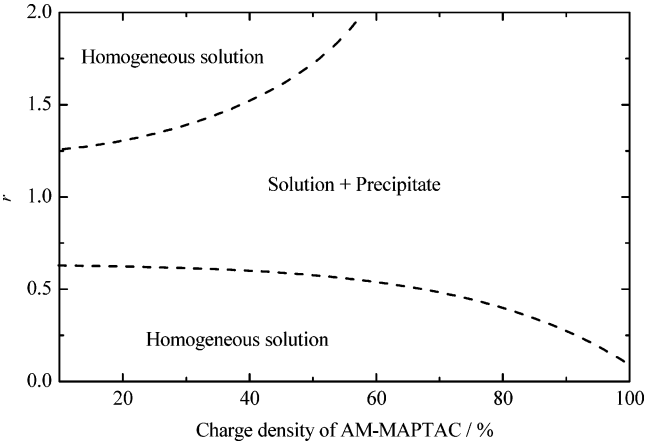

Figure 3. Diagram showing the different phases formed in mixtures of SDS and AM−MAPTAC with different charge densities. The surfactant/polyelectrolyte composition on the *y*-axis is expressed as $r \equiv$ [total charge of SDS-*d*]/[total charge of polyelectrolyte]. The total concentration of polyelectrolyte is always 1 wt %.

phase are dispersed in the aqueous phase and, therefore, it is difficult to completely separate the two phases from each other.

Methods. The small-angle neutron scattering (SANS) experiments were carried out at the D11 SANS instrument at Institut Laue-Langevin (ILL), Grenoble, France. A range of scattering vectors q from 0.003 to 0.2 Å^{-1} were covered by three sample-to-detector distances (1.2, 5.5, and 12 m) at the neutron wavelength of 8 Å. The wavelength resolution was 10% (full width at half-maximum value).

The samples were kept in quartz cells (Hellma) with a path length of 2 mm for samples in D_2O, whereas 1 mm cells were used for the H_2O/D_2O mixtures. The raw data were corrected for background from the solvent, sample cell, and other sources by conventional procedures[23] using standard ILL software. The two-dimensional isotropic scattering spectra were azimuthally averaged and converted to an absolute scale after being corrected for detector efficiency by dividing by the incoherent scattering spectra of pure water measured in a 1 mm cell.[24] The setting with 5.5 m sample-to-detector distance was used as the reference setting for the absolute scale.

Data Analysis. A quantitative estimate of the geometrical structure of the aggregates formed in the transparent isotropic solutions could be obtained by means of fitting our small-angle scattering data to either a model for prolate ellipsoids of revolution or a model for polydisperse rigid rods.[25]

The scattering cross-section for a monodisperse collection of interacting nonspherical particles can be expressed in the following way[25]

$$\frac{d\sigma_m(q)}{d\Omega} = \Delta\rho_m{}^2 M\langle F^2(q)\rangle_0\left[1 + \frac{\langle F(q)\rangle_0{}^2}{\langle F^2(q)\rangle_0}(S(q) - 1)\right] \quad (1)$$

where interactions have been taken into account by means of the decoupling approximation.[26] Here, $\Delta\rho_m$ is the difference in scattering length density per unit mass of solute between particles and solvent and M is the molar mass of a single particle.

For an ellipsoid of revolution the orientational averaged form factor is obtained by means of integrating twice over the square of the amplitude

$$F(q,r) = \frac{3[\sin(qR) - qr\cos(qR)]}{(qR)^3} \quad (2)$$

where $R(a,b,\theta) = \sqrt{a^2\sin^2\theta + b^2\cos^2\theta}$, to yield[27]

$$\langle F^2(q)\rangle_0 = \int_0^{\pi/2} F^2[q,R(a,b,\theta)]\sin\theta\, d\theta \quad (3)$$

$\langle F(q)\rangle_0$ is obtained in an analogous way by integration over the amplitude.

To account for interactions between the micelles, the decoupling approximation[26] in eq 1, valid for particles with moderate deviation from spherical shape, was used together with a structure factor $S(q)$ derived by Hayter and Penfold[28] from the Ornstein−Zernike equation and the rescaled mean spherical approximation (RMSA),[29] with a soft repulsive potential between two macroions surrounded by a diffuse double layer of counterions as calculated from the Poisson−Boltzmann theory.

In some of the samples the micelles were seen to be rather long, and the corresponding data were fitted with a model for polydisperse cylinders. To avoid unreasonably long computation times, we have simplified the model by separating the form factor into one contribution which is due to the length of the micelles $P_{length}(q)$ and one contribution due to the particle cross-section $P_{cs}(q)$. Hence, we have used the following scattering cross-section valid for particles with a length much larger than the cross-sectional dimensions[30]

$$\frac{d\sigma_m(q)}{d\Omega} = \Delta\rho_m{}^2 P_{length}(q)P_{cs}(q)\langle M\rangle_w \quad (4)$$

where $\langle M\rangle_w$ is the weight-average molar mass. The form factor $P_{cs}(q)$ for a circular cross-section with radius R is given by[25,31]

$$P_{cs}(q) = \left(\frac{2B_1(qR)}{qR}\right)^2 \quad (5)$$

where $B_1(x)$ is the Bessel function of first order. Because data above $q = 0.2$ Å^{-1} are missing, it was not possible to obtain any additional information by using a two-shell model or assuming an elliptical cross-section in the analysis.

The scattering function for polydisperse rigid rods can be written as follows

$$P_{length}(q) = \frac{\int N_{rod}(L)\, L^2 S_{rod}(q,L)\, dL}{\int N_{rod}(L)\, L^2\, dL} \quad (6)$$

where $N_{rod}(L)$ is the number distribution of micelles with respect to their length L and the form factor for an infinitely thin rod is given by[32]

$$S_{rod}(q,L) = 2\mathrm{Si}(qL) - \frac{4\sin^2(qL/2)}{(qL)^2} \quad (7)$$

where

$$\mathrm{Si}(x) = \int_0^x \frac{\sin t}{t}\, dt \quad (8)$$

The polydispersity of the micelles is difficult to obtain accurately, in particular because interference from other structures is seen in the scattering data (see further below). Hence, we have roughly set the relative standard deviation to $\sigma_L/\langle L\rangle = 0.7$, that is, somewhere between what is expected for infinitely small rods ($\sigma_L/\langle L\rangle = 0$) and infinitely large rods ($\sigma_L/\langle L\rangle = 1$), that is, rods that are much longer than the cross-sectional diameter.[33] In Table 1 we have chosen to present the results in terms of the

TABLE 1: Results from SANS Data Analyses of the Transparent and Isotropic Samples that Contain Free Aggregates[a]

r	AM−MAPTAC60	AM−MAPTAC30	AM−MAPTAC10
0.125	not measured	$a = 18.9$ $b = 39.7$ $\alpha = 1.7$	$a = 12.8$ $b = 66.1$ $\alpha = 1.3$
0.250	$R = 17.3$ $\langle L \rangle = 362$ $\alpha = 0.8$	$a = 17.8$ $b = 51.6$ $\alpha = 3.0$	$a = 15.1$ $b = 53.6$ $\alpha = 2.3$
0.375	not measured	$a = 16.7$ $b = 68.1$ $\alpha = 3.9$	precipitate + micelles
1.50	precipitate	$R = 15.0$ $\langle L \rangle = 550$ $\alpha = 6.0$	not measured

[a] The data were fitted with a model for either monodisperse prolate ellipsoids of revolution with half axes a and b or polydisperse rigid cylinders with a volume-weighted average length $\langle L \rangle$ and cross-sectional radius R. All spatial dimensions are given in angstroms (Å). The relative standard deviation $\sigma_L/\langle L \rangle$ in the polydisperse cylinder model was roughly fixed to 0.7. The number of micelles per polyelectrolyte molecule α could be calculated from the fit results knowing the surfactant molecular volume and polyelectrolyte molar mass. The agreements of the fits as measured by χ^2 are 1.0 except for SDS/AM−MAPTAC60 with $r = 0.25$ ($\chi^2 = 1.4$) and SDS/AM−MAPTAC30 with $r = 1.5$ ($\chi^2 = 6.6$).

volume-weighted average length $\langle L \rangle$ which is only slightly dependent on the assumed value of $\sigma_L/\langle L \rangle$.

Moreover, because it is difficult to take into account, interparticle interference effects were neglected in the analysis using the model for polydisperse rods. However, because the samples are rather dilute with respect to polyelectrolyte and surfactant (~1 wt %), interparticle interactions are expected to be weak, and it is reasonable to believe that the model in eq 4 is a sufficiently good approximation.

Throughout the data analysis corrections were made for instrumental smearing.[34,35] For each instrumental setting the ideal model scattering curves were smeared by the appropriate resolution function when the model scattering intensity was compared with the measured one by means of least-squares methods. The parameters in the model were optimized by means of conventional least-squares analysis.[36]

Results and Discussion

In samples containing polyelectrolyte with a high charge density, or in samples close to charge neutralization, a phase separation into a precipitate and a clear liquid was observed, whereas lower charged polyelectrolytes in sufficient excess of either surfactant or polyelectrolyte were seen to form a transparent isotropic solution. The appearance of the different samples we have studied is summarized in Figure 3.

Mixtures of MAPTAC and SDS-*d*. In mixtures of MAPTAC (100% charge density) and SDS a white precipitate was seen to form at all compositions measured ($0.25 < r < 1.5$). The measurements were carried out both in D_2O where SDS-*d* is contrast matched (cf. Figure 4) and in a D_2O/H_2O mixture where the polyelectrolyte is contrast matched (cf. Figure 5). In the corresponding SANS data of both solvents a Bragg-like peak due to the internal structure of the precipitate was located at the same position ($q = 0.152$ Å^{-1}) in the two solvents. In recent SAXS measurements we were able to observe three additional peaks and determine the internal structure of the precipitate to be cylindrical micelles packed in a 2D hexagonal pattern with a distance equal to 47.7 Å between two adjacent cylinders.[22] In the lower q-regime, the data behave as $I \propto q^{-4}$ in both solvents which is consistent with the presence of large three-dimensional objects. At $r = 0.25$ and $r = 0.50$ in D_2O (where the surfactant is contrast matched), an extra contribution to the scattering is seen in the regime of 0.05 Å^{-1} < q < 0.1 Å^{-1} indicating the presence of free particles in the isotropic liquid solution coexisting with the precipitate (cf. Figure 4). These particles may be either free polyelectrolyte or rod-shaped SDS micelles covered by polyelectrolyte. However, because the corresponding behavior is absent in the D_2O/H_2O mixture (polyelectrolyte is contrast matched), the free particles must to an overwhelming extent be rich in MAPTAC. Likewise, in the D_2O/H_2O mixture at $r = 1.5$ the presence of either SDS micelles or, possibly, mixed MAPTAC−SDS micelles in the liquid solution coexisting with the precipitate is indicated by the SANS data behavior in the intermediate regime (cf. Figure 5). This is what we recently also found for mixtures of SDS and the cationic polyelectrolyte PCMA which has a similar architecture (linear with small side chains and 100% charge density) to that of MAPTAC.[21] The relative amount of micelles present in these samples is too small for us to accurately determine, and it is not possible to quantify the geometry of the micelles by means of fitting data with a detailed model.

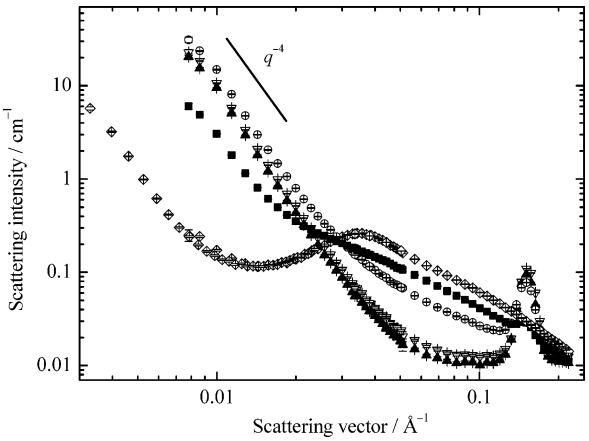

Figure 4. Small-angle neutron scattering intensity as a function of scattering vector q for mixtures of 1 wt % MAPTAC and SDS-*d* in D_2O in which SDS-*d* is contrast matched. The SDS-*d* concentration corresponds to $r = 0$ (diamonds), $r = 0.25$ (squares), $r = 0.50$ (circles), $r = 0.75$ (up triangles), and $r = 1.5$ (down triangles). The $I \propto q^{-4}$ behavior at low q values is consistent with a three-dimensional structure of the aggregates.

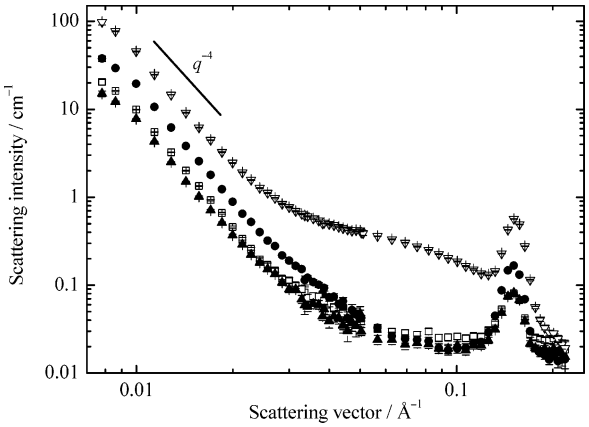

Figure 5. Small-angle neutron scattering intensity as a function of scattering vector q for mixtures of 1 wt % MAPTAC and SDS-*d* in a mixture of $[H_2O]/[D_2O] = 86/14$ in which MAPTAC is contrast matched. The SDS-*d* concentration corresponds to $r = 0.25$ (squares), $r = 0.50$ (circles), $r = 0.75$ (up triangles), and $r = 1.5$ (down triangles).

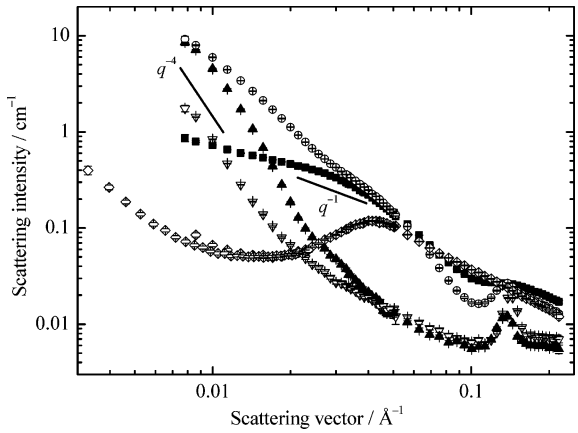

Figure 6. Small-angle neutron scattering intensity as a function of scattering vector q for mixtures of 1 wt % AM−MAPTAC60 and SDS-*d* in D_2O in which SDS-*d* is contrast matched. The SDS-*d* concentration corresponds to $r = 0$ (diamonds), $r = 0.25$ (squares), $r = 0.50$ (circles), $r = 0.75$ (up triangles), and $r = 1.5$ (down triangles).

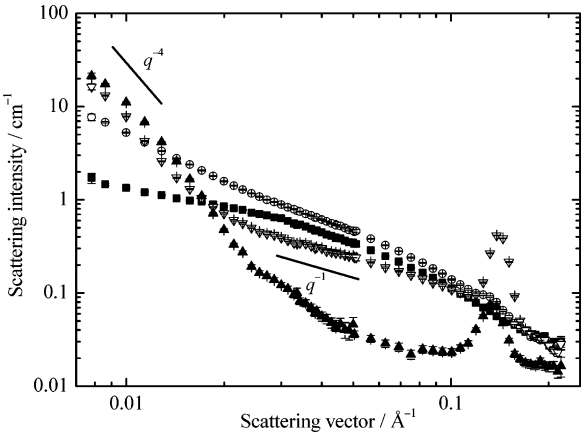

Figure 7. Small-angle neutron scattering intensity as a function of scattering vector q for mixtures of 1 wt % AM−MAPTAC60 and SDS-*d* in a mixture of $[H_2O]/[D_2O] = 82/18$ in which AM−MAPTAC60 is contrast matched. The SDS-*d* concentration corresponds to $r = 0.25$ (squares), $r = 0.50$ (circles), $r = 0.75$ (up triangles), and $r = 1.5$ (down triangles).

In Figure 4 we have also included the data of pure MAPTAC in D_2O. The appearance is typical for a highly charged polyelectrolyte in aqueous solution and in the absence of added salt.[21,37] The scattering behavior can roughly be rationalized as being a product of a form factor, accounting for the particle shape, and a structure factor, accounting for interparticle interactions. The structure factor has a peak corresponding to the characteristic distance between two adjacent polyelectrolyte molecules giving a maximum in the corresponding scattering data in Figure 4. This peak is expected to become less pronounced as the polyelectrolyte charge density decreases. The rise in scattering intensity at low q-values indicates that the polyelectrolyte chains are too large (i.e., radius of gyration larger than about 200 Å) to determine their size from SANS.

Mixtures of AM−MAPTAC60 and SDS-*d*. The scattering data for mixtures of SDS and 60% charged AM−MAPTAC are shown in Figures 6 and 7 for the two solvents where either component is contrast matched. The data appear similar to those of the MAPTAC case for the compositions $r = 0.75$ and $r = 1.5$ with a Bragg-like peak located at $q = 0.138$ Å^{-1} and a q^{-4} behavior at low q-values. From SAXS we found the internal structure to be 2D hexagonal with a distance of 52.6 Å between adjacent cylinders.[22] The presence of free aggregates in the isotropic solution coexisting with a precipitate is clearly seen from the behavior of the spectra at $r = 1.5$ in the D_2O/H_2O mixture (cf. Figure 7).

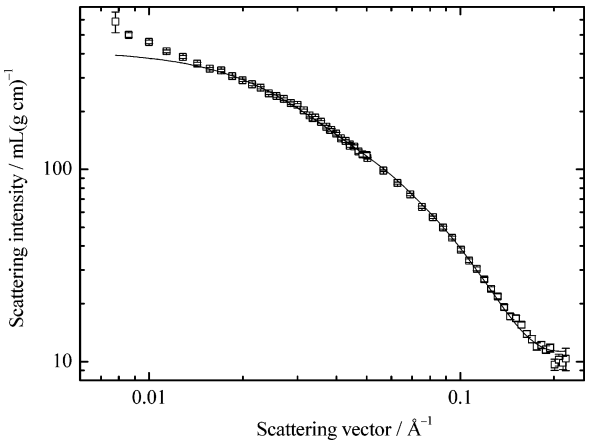

Figure 8. Normalized scattering intensity as a function of scattering vector q for a mixture of SDS-*d* and AM−MAPTAC60 at $r = 0.25$ in a mixture of $[H_2O]/[D_2O] = 82/18$ in which AM−MAPTAC60 is contrast matched. Individual symbols represent data obtained with different combinations of neutron wavelength and sample detector distance. The lines represent the result from a fit between 0.02 Å^{-1} < q < 0.2 Å^{-1} with a model for polydisperse cylinders. The result of the model fit is given in Table 1.

The scattering data for samples with a larger excess of AM−MAPTAC60, that is, $r = 0.25$ and $r = 0.50$, appear very different. For $r = 0.25$ the sample is transparent and the corresponding data for the D_2O/H_2O mixture could be well fitted with a model for polydisperse cylinders above $q = 0.01$ Å^{-1} (cf. Figure 8 and Table 1). As a matter of fact, we find that prolate or rod-shaped micelles are present in all transparent samples investigated in this study (cf. Table 1 and further below) indicating that the cylinders in the hexagonal solid phase have been completely dissolved in the isotropic solution. The scattering data for these samples are, however, completely incompatible with the presence of small spherical micelles.[33,38] A growth of oblate micelles formed by pure SDS in water to longer rods[38] is indeed expected as a result of the lowering of the aggregate charge density as the micelles interact with the oppositely charged polyelectrolyte, the positive charges of which must be located close to the negative charges of the SDS. Moreover, it is indicated by the deviations between the model and the data at low q-values (q < 0.01 Å^{-1}) that small amounts of large objects are present in the solution. We cannot, however, exactly determine the size and shape of these particles from a model fit, but it is reasonable to believe that they consist of small fragments of the same precipitate found in large amounts close to $r = 1$.

From Figures 6 and 7 it is also seen that the data of the transparent samples behave as $I \propto q^{-1}$, typical for rod-shaped micelles, irrespective of whether the surfactant or the polyelectrolyte is contrast matched. This indicates that SDS and the polyelectrolyte form a common structure of rod-shaped micelles. It is reasonable to believe that the polyelectrolytes are wrapped around cylinders of aggregated SDS in such a manner that the positive charges of the former are closely located to the negatively charged surfactant headgroups (cf. Figure 9). As a result, pairs of counterions are released to the bulk solution which is favorable from an entropic point of view. The additional information that may be extracted from the scattering data for samples in D_2O (surfactant is contrast matched) regards the structure of the polymer cross-section which is rather difficult to model with its small side chains attached to the

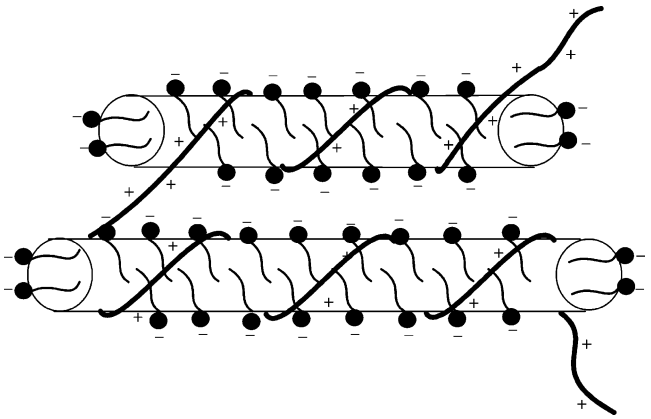

Figure 9. Schematic representation of cylindrical micelles wrapped in polyelectrolyte chains formed in isotropic solutions of 30% and 60% charged AM−MAPTAC and SDS.

polymer backbone. Because this structure is already well-known, we have not analyzed the scattering data for samples in D_2O by means of model fitting.

The number of micelles per polyelectrolyte molecule α could be estimated by calculating the micelle aggregation number from the fit results together with the surfactant molecular volume and comparing the results with the known values of the polyelectrolyte molar mass and surfactant and polyelectrolyte concentrations. The values for α are given in Table 1. The effect of free surfactants was neglected which may affect the results for the lowest SDS concentrations where the overall SDS concentration might not be much larger than the concentration of free SDS. The value of α was found to be close to unity (α = 0.8) for the sample in Figure 8.

The sample at $r = 0.50$ is turbid but appears homogeneous. The corresponding SANS data show the characteristic Bragg-like peaks, demonstrating the presence of large 3-dimensional objects with an internal 2D structure. However, it is evident from data for both solvents that an appreciable amount of free aggregates, containing surfactant as well as polyelectrolyte, is present in the solution. The amount of free aggregates is, however, too small to allow us to quantify their size and shape by means of model fitting.

It may finally be noted that we may exclude the possibility that the scattering behavior as function of polyelectrolyte/surfactant ratio seen in Figures 4 and 6 is only a consequence of reduced interparticle interactions. The latter only influences scattering data in the low *q*-regime as demonstrated in Figure 10 where the effect of screening electrostatic interactions by adding salt is shown.

Mixtures of AM−MAPTAC30 and SDS-*d*. SANS data for mixtures of SDS and 30% charged AM−MAPTAC are plotted in Figures 11 and 12. A noticeable precipitation was only seen at $r = 0.75$. At $r = 0.50$ the sample was turbid, whereas transparent solutions were formed at $r = 0.125$, 0.25, 0.375, and 1.5. The Bragg-like peak for the sample with $r = 0.75$ is located at $q = 0.124$ Å^{-1} corresponding to an interaggregate distance of 58.5 Å. The 2D hexagonal structure has been confirmed from SAXS measurements.[22] The trend of increasing interaggregate distance with decreasing charge density of AM−MAPTAC has been suggested to be mainly the result of an increasing volume of noncharged polyelectrolyte segments incorporated in the surfactant−polyelectrolyte complex. However, it was also found that an appreciable amount of water, favored by entropy of mixing, must be included in the aggregates.[22]

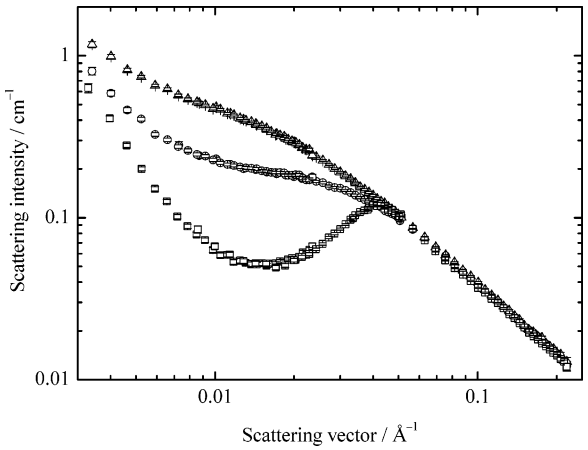

Figure 10. Small-angle neutron scattering intensity as a function of scattering vector *q* for AM−MAPTAC60 at different concentrations of NaCl in D_2O. The salt concentrations are [NaCl] = 0 (squares), [NaCl] = 30 mM (circles), and [NaCl] = 100 mM (triangles).

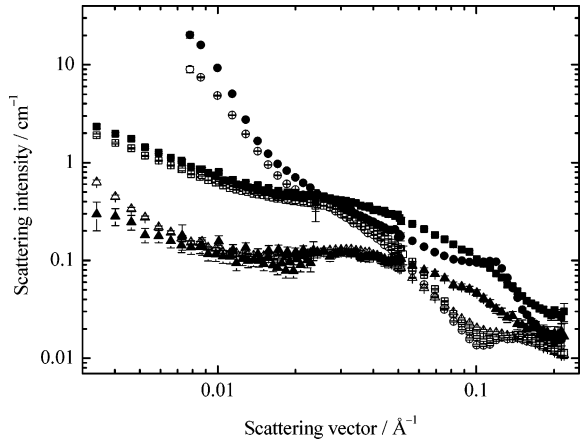

Figure 11. Small-angle neutron scattering intensity as a function of scattering vector *q* for mixtures of 1 wt % AM−MAPTAC30 and SDS-*d* in D_2O (open symbols), in which SDS-*d* is contrast matched, and in a mixture of $[H_2O]/[D_2O] = 77/23$ (filled symbols) in which AM−MAPTAC30 is contrast matched. The SDS-*d* concentration corresponds to $r = 0.125$ (triangles), $r = 0.375$ (squares), and $r = 0.50$ (circles).

The similar scattering behavior for the two solvents at low *q*-values observed at all compositions indicates that surfactant and polyelectrolyte always form a common structure. However, the differences at high *q*-values between the two solvents for samples in excess of polyelectrolyte (cf. Figure 11) show that the local structure for surfactant and polyelectrolyte is different. The scattering behavior of the polyelectrolyte coincides in this regime for the different samples which is expected because it mainly consists of information about the polyelectrolyte cross-section. The corresponding scattering data for the D_2O/H_2O mixture (polyelectrolyte is contrast matched) could be fitted with a model for prolate micelles, and the corresponding results are given in Table 1. Deviations between model and data at $q < 0.01$ Å^{-1}, similar to those seen for the case of AM−MAPTAC60 in Figure 8, indicate the presence of large objects. The major half axis is seen to increase from 39.7 Å at $r = 0.125$ to 68.1 Å at $r = 0.375$, which is expected because the aggregate charge density decreases with increasing *r* below $r = 1$, whereas the minor half axis is a fairly constant 17−19 Å. The average number of micelles per polyelectrolyte increases from 1.7 at $r = 0.125$ to 3.9 at $r = 0.375$. For the turbid sample at $r = 0.50$ a small Bragg-peak is seen in the data in Figure 11 for the $D_2O/$

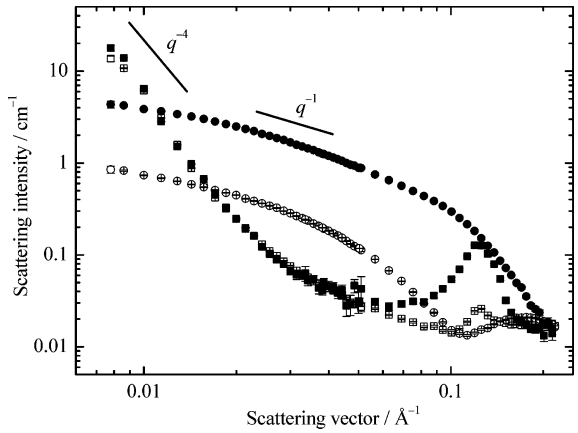

Figure 12. Small-angle neutron scattering intensity as a function of scattering vector q for mixtures of 1 wt % AM−MAPTAC30 and SDS-*d* in D_2O (open symbols), in which SDS-*d* is contrast matched, and in a mixture of $[H_2O]/[D_2O] = 77/23$ (filled symbols) in which AM−MAPTAC30 is contrast matched. The SDS-*d* concentration corresponds to $r = 0.75$ (squares) and $r = 1.5$ (circles).

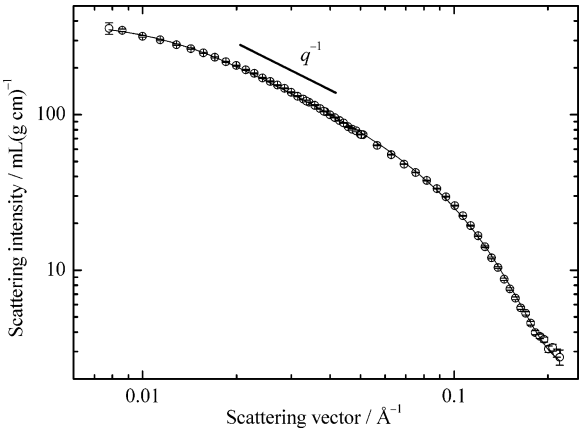

Figure 13. Normalized scattering intensity as a function of scattering vector q for a mixture of SDS-*d* and AM−MAPTAC30 at $r = 1.5$ in a mixture of $[H_2O]/[D_2O] = 77/23$ in which AM−MAPTAC60 is contrast matched. Individual symbols represent data obtained with different combinations of neutron wavelength and sample detector distance. The lines represent the result from a fit with a model for polydisperse cylinders. The result of the model fit is given in Table 1.

H_2O mixture indicating the coexistence of micelles and larger SDS−polyelectrolyte complexes of close-packed cylinders.

The SANS data for the AM−MAPTAC30/SDS mixture at $r = 1.5$ in the D_2O/H_2O mixture could be well fitted with a model for polydisperse cylinders in the entire available q-range (cf. Figure 13). The rod-shaped micelles in excess of SDS are much larger than those in an excess of polyelectrolyte with a weight-average length of $\langle L \rangle = 550$ Å, and the number of micelles per chain is found to be equal to 6. The scattering data for this sample in both solvents behave as $I \propto q^{-1}$ (cf. Figure 12), typical for rod-shaped micelles, indicating the common structure of the SDS−polyelectrolyte aggregates suggested in Figure 9 where a few micelles are connected to each polymer chain.

Mixtures of AM−MAPTAC10 and SDS-*d*. For mixtures of SDS and 10% charged AM−MAPTAC transparent but very viscous solutions form at $r = 0.125$ and $r = 0.250$ where rather small prolate micelles were seen to be present (cf. Figure 14). The fit results for samples in a D_2O/H_2O mixture that contrast matches the polyelectrolyte are given in Table 1. However, because of the low contrast between SDS and solvent, the quality of the data is limited. Similarly to the case of AM−MAPTAC30, the data for the two solvents behave in the same way at low

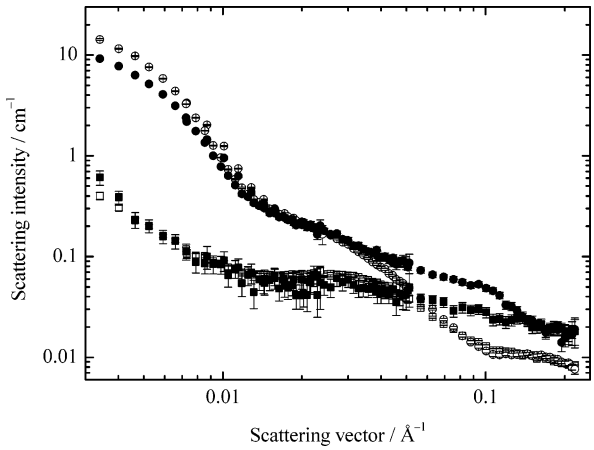

Figure 14. Small-angle neutron scattering intensity as a function of scattering vector q for mixtures of 1 wt % AM−MAPTAC10 and SDS-*d* in D_2O (open symbols), in which SDS-*d* is contrast matched, and in a mixture of $[H_2O]/[D_2O] = 71/29$ (filled symbols) in which AM−MAPTAC10 is contrast matched. The SDS-*d* concentration corresponds to $r = 0.125$ (squares) and $r = 0.375$ (circles).

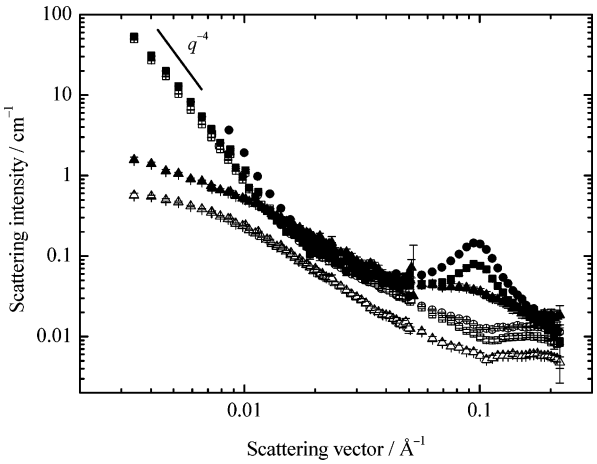

Figure 15. Small-angle neutron scattering intensity as a function of scattering vector q for mixtures of 1 wt % AM−MAPTAC10 and SDS-*d* in D_2O (open symbols), in which SDS-*d* is contrast matched, and in a mixture of $[H_2O]/[D_2O] = 71/29$ (filled symbols) in which AM−MAPTAC10 is contrast matched. The SDS-*d* concentration corresponds to $r = 0.675$ (squares), $r = 0.75$ (circles), and $r = 1.25$ (up triangles).

q-values but are conspicuously different at high q-values. This is expected because mainly the local cross-sectional structure formed by either component contributes and, as a result, the samples where the polyelectrolyte is visible show the same behavior in this regime. The high viscosity of the samples indicates that the small micelles are incorporated in some larger structure, likely connected by polymers in a network-like structure. At $r = 0.375$ the sample is slightly turbid and the scattering data indicate the coexistence of micelles and large complexes.

The scattering data at higher r appear more complicated although a similar behavior at low q-values for the two solvents indicates that SDS and polyelectrolyte still form a common structure (cf. Figure 15). A broad Bragg-like peak at $q = 0.097$ Å^{-1} together with a $I \propto q^{-4}$ behavior at low q-values was seen at $r = 0.675$ and $r = 0.75$ for the solvent mixture, where only the scattering behavior of the surfactant is observed, but is absent in the corresponding samples in D_2O, where only polyelectrolyte is observed. This indicates that the surfactant forms more ordered structures than the polyelectrolyte probably due to the

presence of largely disordered segments of uncharged monomers in the polymer. A similar behavior, but not as evident, could also be seen for the case of AM−MAPTAC30 (cf. Figures 11 and 12).

In the samples in excess SDS ($r = 1.25$ and 1.5) a somewhat turbid gellike structure is observed with the bare eye, and in the corresponding scattering data for the D_2O/H_2O mixture a very broad peak can be vaguely seen at $q \approx 0.1$ Å^{-1} (cf. Figure 15). This indicates that smaller aggregates, possibly rods, are arranged in a larger ordered structure similar to that for the precipitate seen at higher polymer charge densities but with the rods more loosely connected. The structure is, however, too complicated to allow model fitting with a detailed model.

Conclusions

We have investigated aqueous mixtures of (deuterated) SDS and cationic polyelectrolytes (AM−MAPTAC) with different charge densities using small-angle neutron scattering. In mixtures of 100% charged MAPTAC and SDS a phase separation into a precipitate and a clear liquid solution occurs, and from recent small-angle X-ray scattering we could conclude that the precipitate consists of a 2D hexagonal lattice of close-packed cylindrical micelles.[22] Samples of SDS and lower charged polyelectrolyte (AM−MAPTAC10, AM−MAPTAC30, and AM−MAPTAC60), where either SDS or polyelectrolyte is in sufficient excess, are clear and isotropic. The corresponding scattering data indicate that the precipitate has dissolved into rod-shaped micelles that may be connected to each other by polyelectrolyte chains. The micelles are considerably elongated with lengths ranging from 80 to 550 Å. The cross-sectional radius is fairly constant at about 15 Å. The size of the micelles increases rapidly with SDS concentration and also with increasing polyelectrolyte charge density. The number of micelles per chain was seen to be rather close to unity, that is, in the range of 1−6. In some of the samples that appear turbid but homogeneous, the scattering data are consistent with the coexistence of micelles and larger polyelectrolyte−surfactant complexes. In samples with the lower charged AM−MAPTAC10 and SDS the internal structure appears much less ordered with a larger distance between the surfactant aggregates giving it a more gellike structure.

References and Notes

(1) Wei, Y.-C.; Hudson, S. M. *J. Macromol. Sci., Rev. of Macromol. Chem. Phys.* **1995**, *C35*, 15.

(2) Li, Y.; Dubin, P. L. In *Structure and Flow in Surfactant Solutions*; Herb, C. A., Prud'homme, R. K., Eds.; American Chemical Society: Washington, DC, 1994; Vol. 578, p 320.

(3) Goddard, E. D.; Ananthapadmanabhan, K. P. *Interactions of Surfactants with Polymers and Proteins*; CRC Press: Boca Raton, FL, 1993.

(4) Piculell, L.; Lindman, B. *Adv. Colloid Interface Sci.* **1992**, *41*, 149.

(5) Piculell, L.; Guilemet, F.; Thuresson, K.; Shubin, V.; Ericsson, O. *Adv. Colloid Interface Sci.* **1996**, *63*, 1.

(6) Kwak, J. C. T. *Polymer-Surfactant Systems*; Marcel Dekker, Inc.: New York, 1998; Vol. 77.

(7) Iliopoulos, I. *Curr. Opin. Colloid Interface Sci.* **1998**, *3*, 493.

(8) Cosgrove, T.; White, S. J.; Zarbakhsh, A.; Heenan, R. K.; Howe, A. M. *Langmuir* **1995**, *11*, 744.

(9) Cabane, B.; Duplessix, R. *J. Phys. (Paris)* **1982**, *43*, 1529.

(10) Cabane, B.; Duplessix, R. *Colloids Surf.* **1985**, *13*, 19.

(11) Antonietti, M.; Conrad, J.; Thünemann, A. *Macromolecules* **1994**, *27*, 6007.

(12) Antonietti, M.; Kaul, A.; Thünemann, A. *Langmuir* **1995**, *11*, 2633.

(13) Antonietti, M.; Burger, C.; Effing, J. *Adv. Mater.* **1995**, *7*, 751.

(14) Antonietti, M.; Wenzel, A.; Thünemann, A. *Langmuir* **1996**, *12*, 2111.

(15) Antonietti, M.; Maskos, M. *Macromolecules* **1996**, *29*, 4199.

(16) Merta, J.; Torkkeli, M.; Ikonen, T.; Serimaa, R.; Stenius, P. *Macromolecules* **2001**, *34*, 2937.

(17) Ilekti, P.; Piculell, L.; Tournilhac, F.; Cabane, B. *J. Phys. Chem. B* **1998**, *102*, 344.

(18) Ilekti, P.; Martin, T.; Cabane, B.; Piculell, L. *J. Phys. Chem. B* **1999**, *103*, 9831.

(19) Svensson, A.; Piculell, L.; Cabane, B.; Ilekti, P. *J. Phys. Chem. B* **2002**, *106*, 1013.

(20) Zhou, S.; Hu, H.; Burger, C.; Chu, B. *Macromolecules* **2001**, *34*, 1772.

(21) Claesson, P. M.; Bergström, M.; Dedinaite, A.; Kjellin, M.; Legrand, J. F.; Grillo, I. *J. Phys. Chem. B* **2000**, *104*, 11689.

(22) Bergström, M.; Kjellin, U. R. M.; Claesson, P. M.; Pedersen, J. S.; Nielsen, M. M. *J. Phys. Chem. B* **2002**, *106*, 11412.

(23) Cotton, J. P. *Neutron, X-ray and Light Scattering: Introduction to an Investigative Tool For Colloidal and Polymeric Systems*; Lindner, P., Zemb, T., Eds.; Elsevier/North Holland: Amsterdam, 1991.

(24) Wignall, G. D.; Bates, F. S. *J. Appl. Crystallogr.* **1986**, *20*, 28.

(25) Pedersen, J. S. *Adv. Colloid Interface Sci.* **1997**, *70*, 171.

(26) Kotlarchyk, M.; Chen, S. H. *J. Chem. Phys.* **1983**, *79*, 2461.

(27) Guiner, A. *Ann. Phys.* **1939**, *12*, 161.

(28) Hayter, J. B.; Penfold, J. *Mol. Phys.* **1981**, *42*, 409.

(29) Hansen, J. P.; Hayter, J. B. *Mol. Phys.* **1982**, *46*, 651.

(30) Pedersen, J. S.; Schurtenberger, P. *J. Appl. Crystallogr.* **1996**, *29*, 646.

(31) Pedersen, J. S.; Egelhaaf, S. U.; Schurtenberger, P. *J. Phys. Chem.* **1995**, *99*, 1299.

(32) Neugebauer, T. *Ann. Phys. (Leipzig)* **1943**, *42*, 509.

(33) Bergström, M.; Pedersen, J. S. *J. Phys. Chem. B* **1999**, *103*, 8502.

(34) Pedersen, J. S. *J. Phys. IV (Paris) Colloq. C8* **1993**, *3*, 491.

(35) Pedersen, J. S.; Posselt, D.; Mortensen, K. *J. Appl. Crystallogr.* **1990**, *23*, 321.

(36) Bevington, B. R. *Data Reduction and Error Analysis for Physical Sciences*; McGraw-Hill: New York, 1969.

(37) Förster, S.; Schmidt, M. *Adv. Polym. Sci.* **1995**, *120*, 51.

(38) Bergström, M.; Pedersen, J. S. *Phys. Chem. Chem. Phys* **1999**, *1*, 4437.